HHS Public Access

Author manuscript

Science. Author manuscript; available in PMC 2017 August 29.

Published in final edited form as:

Science. 2016 June 10; 352(6291): 1341–1344. doi:10.1126/science.aaf6419.

Zebrafish model of idiopathic scoliosis link cerebrospinal fluid flow to defects in spine curvature

D. T. Grimes[1,*], **C. W. Boswell**[2,*], **N. F. C. Morante**[1,*], **R. M. Henkelman**[3], **R. D. Burdine**[1], and **B. Ciruna**[2,†]

[1]Department of Molecular Biology, Princeton University, Washington Road, Princeton, NJ 08544, USA

[2]Program in Developmental & Stem Cell Biology, The Hospital for Sick Children, 686 Bay Street, Toronto, Ontario, M5G 0A4, Canada; Department of Molecular Genetics, The University of Toronto, Toronto, Ontario, M5S 1A8, Canada

[3]Mouse Imaging Centre (MICe), The Hospital for Sick Children, 25 Orde Street, Toronto, Ontario, M5T 3H7, Canada; Department of Medical Biophysics, The University of Toronto, Toronto, Ontario, M5G 2M9, Canada

Abstract

Idiopathic scoliosis (IS) affects 3% of children worldwide, yet mechanisms underlying spinal deformity remain unknown. Here we show that *ptk7* mutant zebrafish, a faithful genetic model of IS, exhibit ependymal cell (EC) cilia development and cerebrospinal fluid (CSF) flow defects. Transgenic re-introduction of Ptk7 in motile ciliated lineages prevents scoliosis in *ptk7* mutants, while mutation of multiple independent cilia motility genes yield IS phenotypes. We define a finite developmental window for motile cilia in spine morphogenesis. Notably, restoration of cilia motility, after scoliosis onset, blocks spinal curve progression. Together, our results indicate a critical role for cilia-driven CSF flow in spine development, implicate irregularities in CSF flow as an underlying biological cause of IS and provide proof-of-principle that non-invasive therapeutic intervention could prevent severe scoliosis.

Main Text

Idiopathic scoliosis (IS) is a complex genetic disorder characterized by three-dimensional spinal curvatures, which arise in the absence of observable physiological or anatomical defects. Commonly diagnosed during adolescence, IS can cause disfigurement, reduced respiratory and pulmonary function, as well as chronic pain (1). Unlike congenital or neuromuscular forms of scoliosis, in which spinal curves develop from vertebral malformations and/or underlying morbidities of the musculature and nervous system, the

†Corresponding author. ciruna@sickkids.ca.
*These authors contributed equally

Author Contributions: DTG, CWB, and NFCM performed all experiments characterizing scoliosis phenotypes. CWB cloned and characterized *foxj1a* transgenic lines. NFCM generated the *dyx1c1*^{pr13} allele. CWB and RMH performed μCT. BC and CWB performed SEM and CSF flow analyses. DTG, CWB, NFCM, RDB, and BC analyzed the data. DTG, CWB and BC wrote the manuscript and all authors read and edited the manuscript.

biological cause of IS remains unknown. As a result, treatment is limited to managing spinal deformity post-onset, through bracing and/or corrective surgery (1).

Genome-wide association studies have identified IS-associated polymorphisms in divergent human populations, but phenotypic and genetic variability have made it difficult to define causative mutations (1). Furthermore, a historical lack of appropriate animal models has confounded our basic understanding of the biology underlying IS (2). However, teleosts (bony fish) are naturally prone to idiopathic spinal curvature (3) and recent genetic studies have identified faithful zebrafish IS models, providing important insights into the genetic causes of scoliosis (4, 5) as well as a means to functionally validate human IS-associated genetic variants (4, 6, 7). Notably, studies of zebrafish protein tyrosine kinase-7 (*ptk7*) mutants, which present all defining attributes of human disease, have implicated dysregulated Wnt signaling in the pathogenesis of IS (4).

Ptk7 is an essential regulator of both canonical Wnt/β-catenin and non-canonical Wnt/planar cell polarity (PCP) signaling pathways (8). Although defects in either pathway are associated with a myriad of developmental abnormalities, both PCP and Wnt/β-catenin signaling have been implicated in the function of cilia (9–11). Cilia are microtubule-based organelles that project into the extracellular space and play critical roles in the perception and integration of environmental signals (12, 13). Although most cell types elaborate short primary cilia, longer motile cilia are present on the surface of specialized cells and function to generate directional extracellular fluid flow in several contexts. Cilia-directed flow within early embryonic organizers breaks left-right (L-R) symmetry (14) and CSF flow, which is critical for central nervous system homeostasis (15), is generated by the polarized beating of EC cilia lining brain ventricles (16). Notably, abnormal L-R asymmetries and defective CSF flow have been observed in IS patients (17) and an elevated incidence of scoliosis has been documented among primary ciliary dyskinesia (PCD) patients (18). We therefore hypothesized that motile cilia dysfunction may contribute to the etiopathogenesis of IS.

To test this, we first investigated EC motile cilia structure and function in scoliotic *ptk7* mutant zebrafish and sibling *ptk7*/+ controls. Examination of *ptk7* mutant brain ventricles by scanning electron microscopy (SEM) revealed severe hydrocephalus (Fig. 1A,B), a phenotype commonly associated with loss of EC cilia function (16). Moreover, whereas a dense network of polarized EC cilia lined the ventral surface of *ptk7*/+ ventricles, cilia in *ptk7* mutant ventricles were sparse and, when present, lacked posterior polarization (Fig. 1A′,B′). To directly examine the consequence of EC cilia defects, we tracked fluorescent microsphere movement across the ventral surface of the rhombencephalic ventricle (Fig. 2A). Dynamic anterior-to-posterior flow was observed across the ventricle of *ptk7*/+ brains (Fig. 2B,G; Movie S1). In contrast, although some movement was observed during particle tracking in *ptk7* mutants, microspheres exhibited irregular trajectories and significantly reduced speeds (Fig. 2C,G; Movie S2). These results demonstrate abnormal CSF flow within the ventricular system of scoliotic *ptk7* mutants and are consistent with a role for EC motile cilia defects in the etiology of IS.

To investigate whether scoliosis specifically results from motile cilia dysfunction, we assessed potential rescue of *ptk7* mutant spinal curves following transgenic re-introduction

of wild-type Ptk7 in motile ciliated cell lineages only. The transcription factor FoxJ1a is a master regulator of motile ciliogenesis (19). We therefore cloned and characterized a *foxj1a* enhancer element that specifically drives transgene expression in all known sites of motile cilia formation, as demonstrated in multiple *foxj1a::eGFP* transgenic lines (Fig. S1A–D; Movie S3). Notably, along the trunk of juvenile animals, Tg(*foxj1a::eGFP*) expression was predominantly restricted to midline structures of the brain and spinal cord. We next generated four independent *foxj1a::ptk7* stable transgenic lines (Fig. S1E) and found that the presence of Tg(*foxj1a::ptk7*) restored EC cilia and also rescued hydrocephalus and CSF flow defects in *ptk7* mutant fish (Figs. 1C,C′, 2D,G; Movie S4). Importantly, spinal curve formation, assessed by micro-computed tomography (μCT), was also fully rescued by the transgenes (n=59/59; Fig. 1D–E′), showing that scoliosis in mutants is specifically caused by Ptk7 dysfunction in motile ciliated lineages.

If cilia motility defects contribute to IS pathogenesis, then zebrafish *ccdc40* (20), *ccdc151* (21), *dyx1c1* (22) and *c21orf59* (23) mutations, which all disrupt cilia motility, should develop scoliosis. However, aberrant cilia motility causes a characteristic suite of embryonic phenotypes that usually result in death by 1–2 weeks of development (20, 21), precluding analysis of adolescent spine formation. To circumvent this early lethality, we utilized two strategies. First, we took advantage of the *c21orf59* temperature sensitive mutation *tm304*, here called $c21orf59^{TS}$ (24). At 30°C (restrictive temperature), $c21orf59^{TS}$ mutant embryos exhibit abnormal cilia motility and associated developmental defects (Fig. 3A,B). However, at 25°C (permissive temperature), $c21orf59^{TS}$ embryos retain cilia motility and can develop normally (Fig. 3C) (24). Notably, $c21orf59^{TS}$ mutants raised at 25°C for 5 days to rescue embryonic defects and then shifted to 30°C appear wild-type through juvenile stages, exhibiting normal vertebral formation as monitored using the vital fluorescent Ca^{2+}-binding chromophore calcein (Fig. 3D,E). Strikingly, CSF flow in the rhombencephalic ventricle of these $c21orf59^{TS}$ mutants was severely compromised (Fig. 2E,G; Movie S5). Moreover, all mutant fish develop spinal curves that begin during late larval stages (3–4 weeks of age; Fig. S2A,B) and model defining attributes of IS (Fig. 3F–I; Movie S6).

Our second strategy involved rescuing embryonic phenotypes by RNA injections at the 1-cell stage and analyzing mutants during adolescence. Using CRISPR/Cas9 gene targeting, we generated a *dyx1c1* mutant allele (Fig. S3). Functional characterization of *dyx1c1* mutants revealed abnormal cilia motility and associated developmental defects including embryonic lethality (Fig. S3C–F) in agreement with gene knockdown studies (22). Strikingly, *dyx1c1* mutants, rescued through embryogenesis by wild-type *dyx1c1* mRNA injection, developed severe 3-dimensional spinal curvatures in the absence of congenital vertebral malformations (Fig. 3J; Fig. S2A–B, S4). Furthermore, *ccdc151* and *ccdc40* mutant embryos rescued through embryonic stages also developed late-onset spinal curves that model IS (Fig. 3K,L). Our demonstration that mutations in four different genes, each of which has been characterized to disrupt cilia motility, all yield similar adolescent spinal curve phenotypes provides strong evidence that motile cilia dysfunction represents the underlying cell biological cause of IS in these models.

These experiments further demonstrate a post-embryonic requirement for motile cilia in spine morphogenesis. Indeed, transient knock-down of Dyx1c1 or Ccdc151 through only the

first 3–4 days of embryogenesis (by injection of translation blocking antisense morpholino oligonucleotides (MOs)) does not result in adolescent spinal curvatures despite the fact that MO-injected embryos phenocopy genetic mutants during early embryogenesis (Fig. S5). To define the critical developmental window for motile cilia function in the etiopathogenesis of IS, we performed a series of temperature shift experiments using the *c21orf59*^{TS} mutant allele. *c21orf59*^{TS} mutant embryos were raised at 25°C for at least 5 days (to rescue embryonic phenotypes), transferred to a restrictive temperature (30°C) at defined incremental stages of development and screened for spinal curvatures at sexual maturity (Fig. 4A–D). *c21orf59*^{TS} mutants shifted to restrictive temperatures at 19 dpf all developed severe spinal curves by 5 weeks of age (Fig. 4A,E). By contrast, *c21orf59*^{TS} mutants shifted to 30°C at 24 and 29 dpf exhibited milder spinal curvatures (Fig. 4B,C,E), while all *c21orf59*^{TS} mutants shifted to 30°C at 34 dpf displayed no signs of scoliosis through adult stages (Fig. 4D,E). These results indicate a finite and temporally defined requirement for motile cilia function during spine morphogenesis. This interval correlates with documented periods of accelerated adolescent growth (4) when spinal curves typically manifest in IS.

Finally, to determine whether restoration of motile cilia function can prevent severe spinal curve progression following the onset of scoliosis, we performed restrictive-to-permissive temperature shifts at defined time points. *c21orf59*^{TS} mutant embryos were first raised at 25°C until 7 dpf to rescue embryonic development, transferred to 30°C until the onset of spinal curve formation, and then returned to permissive temperatures at incremental stages of spinal curve progression (Fig. 4F–H). Remarkably, restoration of motile cilia activity at the onset of scoliosis blocks spinal curve progression (Fig. 4J–K). This provides a proof-of-principle that development of severe IS spinal curvatures can be managed without invasive surgical manipulation.

The data presented here demonstrate that cilia motility is required for zebrafish spine morphogenesis. Given the acute hydrocephalus and EC cilia defects observed in *ptk7* mutants, the predominant expression of *foxj1a* rescue transgenes throughout the brain and spinal cord of juvenile animals, plus severe CSF flow defects observed across zebrafish IS models, we suggest that irregularities in CSF flow represent the underlying cell biological cause of IS. Several observations support this model: i) disruption of CSF activity via Kaolin injection into the subarachnoid space can cause scoliosis in both dog and rabbit models (25, 26); and ii) scoliosis is highly prevalent in multiple human conditions associated with obstructed CSF flow, including Chiari malformation, syringomyelia and myelomeningoceles (27–29). Our data can now explain these observations and further implies an evolutionarily conserved role for CSF flow in spine morphogenesis, thus warranting re-examination of the anatomy, physiology and genetics of CSF flow in human IS. Downstream of CSF flow, molecular mechanisms influencing spine morphogenesis remain to be determined but could involve multiple gene products previously associated with IS (*i.e.* potential motile cilia functions for the centriolar protein POC5 (6), or chondrocyte-specific activation of GPR126 (30)). Ultimately, our demonstration that severe spinal curvatures can be prevented with the restoration of motile cilia activity may have significant therapeutic ramifications; pharmaceutical manipulation of the production and/or downstream interpretation of CSF signals could potentially stop severe spinal curve progression in some IS patients, even following the onset/clinical diagnosis of scoliosis.

Supplementary Material

Refer to Web version on PubMed Central for supplementary material.

Acknowledgments

We gratefully acknowledge Eunice Lee, Doug Holmyard, Paul Paroutis and Lisa Yu for technical assistance; Angela Morley, Allen Ng, Cori Hasty, Derrick Bosco and Philip Johnson for zebrafish care; and Jodi Schottenfeld-Roams and Tse-sheun Ku for initial observations of spine curvatures in c21orf59^{TS} mutant fish. This work was supported in part by funding from the Canada Research Chairs program to R.M.H and B.C.; NICHD grant 2R01HD048584 to R.D.B.; and Canadian Institutes of Health Research (MOP-111075) and March of Dimes Foundation (#1-FY13-398) grants to B.C.

References and Notes

1. Cheng JC, et al. Nature Reviews Disease Primers. 2015:15030.
2. Janssen MM, et al. Spine J. 2011; 11:347–358. [PubMed: 21474088]
3. Gorman KF, Breden F. Med Hypotheses. 2009; 72:348–352. [PubMed: 19070438]
4. Hayes M, et al. Nat Commun. 2014; 5:4777. [PubMed: 25182715]
5. Buchan JG, et al. Dev Dyn. 2014; 243:1646–1657. [PubMed: 25283277]
6. Patten SA, et al. J Clin Invest. 2015
7. Sharma S, et al. Nat Commun. 2015; 6:6452. [PubMed: 25784220]
8. Hayes M, et al. Development. 2013; 140:1807–1818. [PubMed: 23533179]
9. Park TJ, et al. Nat Genet. 2008; 40:871–879. [PubMed: 18552847]
10. Borovina A, Superina S, Voskas D, Ciruna B. Nat Cell Biol. 2010; 12:407–412. [PubMed: 20305649]
11. Caron A, Xu X, Lin X. Development. 2012; 139:514–524. [PubMed: 22190638]
12. Singla V, Reiter JF. Science. 2006; 313:629–633. [PubMed: 16888132]
13. Goetz SC, Anderson KV. Nat Rev Genet. 2010; 11:331–344. [PubMed: 20395968]
14. Essner JJ, et al. Nature. 2002; 418:37–38. [PubMed: 12097899]
15. Simon MJ, Iliff JJ. Biochim Biophys Acta. 2016; 1862:442–451. [PubMed: 26499397]
16. Lee L. J Neurosci Res. 2013; 91:1117–1132. [PubMed: 23686703]
17. Wang WJ, et al. J Pediatr Orthop. 2011; 31:S14–27. [PubMed: 21173615]
18. Engesaeth VG, Warner JO, Bush A. Pediatr Pulmonol. 1993; 16:9–12. [PubMed: 8414746]
19. Choksi SP, Lauter G, Swoboda P, Roy S. Development. 2014; 141:1427–1441. [PubMed: 24644260]
20. Becker-Heck A, et al. Nat Genet. 2011; 43:79–84. [PubMed: 21131974]
21. Hjeij R, et al. Am J Hum Genet. 2014; 95:257–274. [PubMed: 25192045]
22. Tarkar A, et al. Nat Genet. 2013; 45:995–1003. [PubMed: 23872636]
23. Austin-Tse C, et al. Am J Hum Genet. 2013; 93:672–686. [PubMed: 24094744]
24. Jaffe KM, et al. Cell Rep. 2016; 14:1841–1849. [PubMed: 26904945]
25. Chuma A, et al. Spine (Phila Pa 1976). 1997; 22:589–594. discussion 595. [PubMed: 9089930]
26. Turgut M, et al. Neurosurg Rev. 2005; 28:289–297. [PubMed: 15931513]
27. Milhorat TH, et al. Neurosurgery. 1999; 44:1005–1017. [PubMed: 10232534]
28. Ozerdemoglu RA, Denis F, Transfeldt EE. Spine (Phila Pa 1976). 2003; 28:1410–1417. [PubMed: 12838099]
29. Verhoef M, et al. Dev Med Child Neurol. 2004; 46:420–427. [PubMed: 15174535]
30. Karner CM, et al. Hum Mol Genet. 2015; 24:4365–4373. [PubMed: 25954032]
31. Kimmel CB, et al. Dev Dyn. 1995; 203:253–310. [PubMed: 8589427]
32. Kwan KM, et al. Dev Dyn. 2007; 236:3088–3099. [PubMed: 17937395]

33. Jao LE, Wente SR, Chen W. Proc Natl Acad Sci U S A. 2013; 110:13904–13909. [PubMed: 23918387]

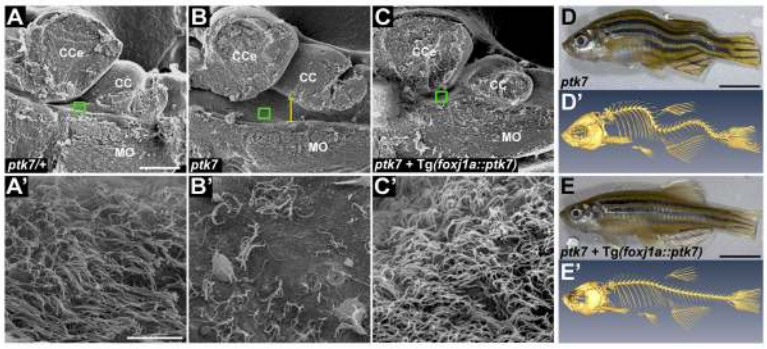

Fig. 1. *ptk7* mutant fish exhibit hydrocephalus, EC cilia defects and spinal curves that are rescued by transgenic re-introduction of *ptk7* specifically in motile ciliated cell lineages

(**A–C**) Representative sagittal images of 2.5 month old *ptk7*/+ (A; n=6), *ptk7* mutant (B; n=6) and *ptk7* mutant expressing Tg(*foxj1a::ptk7*) (C; n=6) brains by SEM. Yellow line (B) demarcates hydrocephalus. Green squares depict corresponding high-magnification SEM images (**A′–C′**). (**D–E′**) Lateral views of fixed (D,E) and μCT rendered (D′,E′) representative adult *ptk7* mutant (D and D′) and *ptk7* mutant expressing Tg(*foxj1a::ptk7*) (E-E′). CCe - corpus cerebelli; CC - crista cerebellaris; MO - medulla oblongata. Scale bars: 250 μm (A,B,C); 10 μm (A′,B′,C′) and 5 mm (D,E).

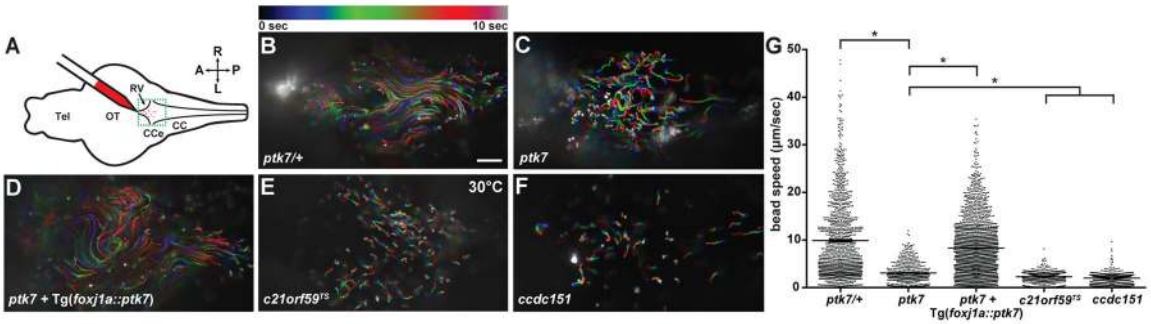

Fig. 2. CSF flow is compromised in zebrafish IS models

(**A**) Schematic of ventricular flow assay in whole-mount adult brains. Green dashed box represents area imaged. (**B** and **C**) Bulk trajectory patterns of beads in whole-mount adult brains in *ptk7* mutants (C) and *ptk7*/+ controls (B). Trajectory paths are color-coded to represent initial position (blue) and final position (red) over 10 seconds. (**D**) Trajectory pattern of *ptk7* mutants expressing Tg(*foxj1a::ptk7*). (**E** and **F**) Trajectory patterns in additional IS models. (**G**) Quantification of CSF flow in various IS models and controls with data points representing an individual bead speed. Bars represent mean with standard error of the mean. Comparisons between genotypes used a *t-test* with * demarcating $p<0.0001$. A - anterior; CCe - corpus cerebelli; CC - crista cerebellaris; L - left; MO - medulla oblongata, OT - optic tectum; P - posterior; RV - rhombencephalic ventricle; R - right; Tel - telencephalon. Scale bar: 50 μm (B).

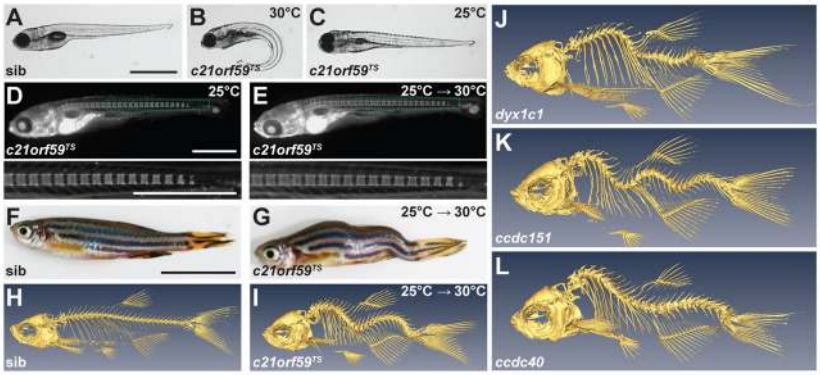

Fig. 3. Cilia motility mutants exhibit spinal curves

(**A–C**) Mutant larvae from *c21orf59*^{TS} intercrosses at 3 dpf exhibited cilia motility-associated defects including ventral axis curvature at 30°C (B) but not at 25°C (C). Sibling (sib) controls had no phenotype (A). (**D** and **E**) Calcein staining of *c21orf59*^{TS} mutants rescued through embryogenesis revealed no vertebral malformations during larval stages at either restrictive (E, n=7) or permissive (D, n=4) temperatures. (**F** and **G**) *c21orf59*^{TS} mutants raised at 25°C until 5 dpf then shifted to 30°C exhibited spinal curves at sexual maturity (G, n=10) that were not present in sib controls (F, n=3). (**H** and **I**) μCT of sib control (H, n=3) and *c21orf59*^{TS} mutants raised at 25°C until 5 dpf then shifted to 30°C (I, n=10). **(J–L)** μCTs of *dyx1c1* mutants (J, n=3), *ccdc151* mutants (K, n=7) and *ccdc40* (L, n=3) mutants, rescued through embryonic stages via injection of wild-type mRNA at the one-cell stage. Scale bars: 1 mm (A and D) and 1 cm (F).

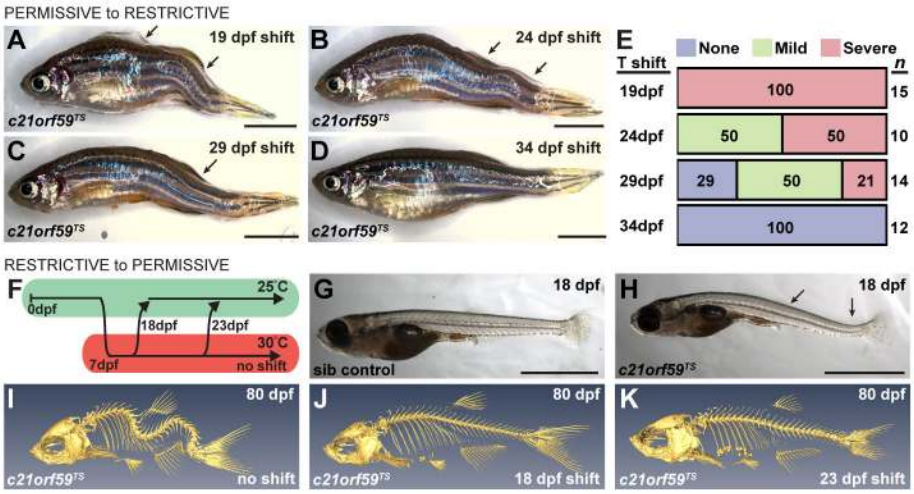

Fig. 4. Temporal window for motile cilia function in spine development

(A–D) Representative lateral views of *c21orf59*^{TS} mutants shifted from 25°C to 30°C at (A) 19 dpf, (B) 24 dpf, (C) 29 dpf and (D) 34 dpf. (**E**) Quantification of scoliosis phenotypes following temperature shift, observed at 6 months post fertilization. (**F**) Schematic of *c21orf59*^{TS} mutant restrictive (30°C) to permissive (25°C) temperature shift experiments. (**G** and **H**) Lateral images of juvenile *c21orf59*^{TS} mutant (H) and sib controls (G) kept at 30°C show curve initiation in mutants by 18 dpf. (**I**) Representative μCT image of 80 dpf unshifted *c21orf59*^{TS} mutants **(J** and **K)** Representative μCT images of 80 dpf *c21orf59*^{TS} mutants shifted from 30°C to 25°C at 18 dpf (J; n=6) or at 23 dpf (K; n=6). Scale bars: 5 mm (A–D) and 2 mm (G–H).